Jet-calculus approach including coherence effects

L. M. Jones
Physics Department, University of Illinois, 1110 West Green Street, Urbana, Illinois 61801

R. Migneron and K. S. S. Narayanan
Department of Applied Mathematics, University of Western Ontario, London, Ontario, Canada N6A 5B9
(Received 8 July 1985; revised manuscript received 23 June 1986)

We show how integrodifferential equations typical of jet calculus can be combined with an averaging procedure to obtain jet-calculus-based results including the Mueller interference graphs. Results in longitudinal-momentum fraction x for physical quantities are higher at intermediate x and lower at large x than with the conventional "incoherent" jet calculus. These results resemble those of Marchesini and Webber, who used a Monte Carlo approach based on the same dynamics.

I. INTRODUCTION

Over the past few years, a great deal of attention has been paid to the predictions of perturbative quantum chromodynamics, especially in the production of jets of hadrons in hard processes.[1–3] Our present understanding of how a quark (gluon) decays in QCD is based on the semiclassical picture developed by Altarelli and Parisi.[4] This was generalized by Konishi, Ukawa, and Veneziano[5] (KUV) into a "jet calculus"—a set of rules for calculating inclusive distributions in x, the longitudinal-momentum fraction. In this calculus, all dominant collinear logarithms come from skeleton tree diagrams with no interference, and thus a probabilistic picture becomes possible. The jet calculus, however, has the defect that the (two or more) partons whose momenta are described may be from widely separated regions in rapidity. To circumvent this problem, Amati and Veneziano[6] introduced the concept of preconfinement, whereby colorless clusters of finite mass can be detected already in the perturbative evolution of partons. Bassetto, Ciafaloni, and Marchesini[7] (BCM) used this idea to define color-connected propagators and the distributions for the quark and the antiquark in a colorless cluster (CC) emitted by a jet.

Improvement in a different direction was made by Crespi and Jones[8] (CJ) who incorporated the momentum of the gluons into the x distribution of the cluster. These equations along with the BCM equations were solved by Jones and Migneron[9] (JM), who implemented the prescription given by Amati *et al.*[10] for improved infrared behavior.

In addition, Mueller[11] has shown that in the leading-logarithm approximation (LLA) the angles at which gluons are emitted in a cascade are ordered. This has substantial consequences for the computation of multiplicities and other quantities which depend in an essential way on the behavior of distributions at low x (Refs. 12 and 13). However, the only actual calculation of detailed consequences which has appeared so far is a Monte Carlo approach developed by Marchesini and Webber[13,14] (MW). As will be clear from the discussion below, this is because it is difficult to rewrite the jet calculus using the angular ordering condition.[11–13] In this paper we discuss the effect of Mueller's observation on the CJ equations and its physical consequences.

Our calculation has the new feature that we use the jet-calculus equations, rather than the Monte Carlo approach

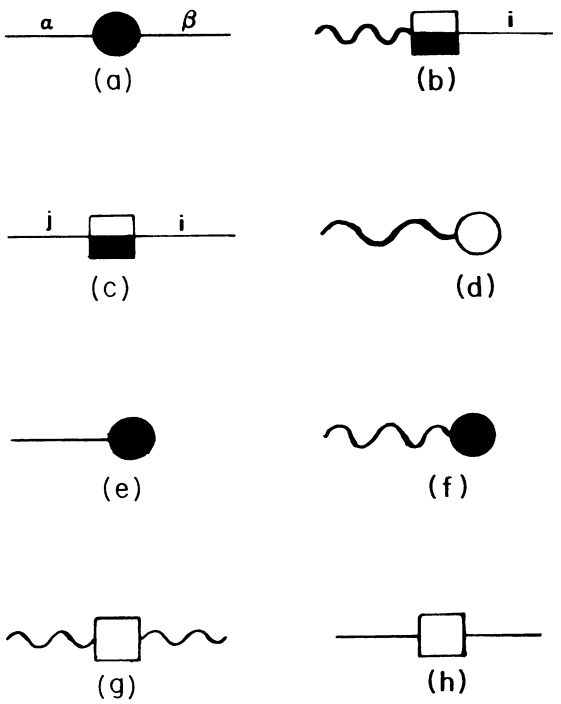

FIG. 1. (a) KUV symbol for $D_\alpha^\beta(Q^2,Q_0^2,x)$, the probability of finding parton β with momentum fraction x at Q_0^2 if one starts with parton α at Q^2. (b) CJ symbol for $H_g^i(Q^2,Q_0^2,x)$. (c) CJ symbol for $H_j^i(Q^2,Q_0^2,x)$. (d) $\sigma_g(Q^2,Q_0^2)$, the probability that gluons only produce gluons. (e) Probability that a quark decays in any way ($=1$). (f) Probability that a gluon decays in any way ($=1$). (g) Representation of virtual potential for a gluon, see text Eq. (2.2a). (h) Representation of virtual potential for a quark, see Eq. (2.2b).

of MW. We rewrite the jet calculus using a kinematic variable appropriate to angular ordering, similar to the procedure used by MW to rewrite the Monte Carlo approach. We then solve the new equations, obtaining results in this new variable. In order to compare with the results in the older variable, an averaging process is introduced which relates the new variable to the old one. Results in longitudinal-momentum fraction x for physical quantities are higher at intermediate x and lower at large x than with the conventional jet calculus.

The outline of the paper is as follows. In Sec. II we review the CJ formalism. In Sec. III we discuss the soft-gluon effects, and the changes that they necessitate in the CJ equations. The interpretation of the revised equations is considered in Sec. IV. Section V contains a discussion of the results, and comparison with previous work. In Sec. VI we present the summary and conclusion.

II. CRESPI-JONES FORMALISM (Ref. 8)

In this approach, one defines new propagators H_g^i and H_j^i which measure the momentum of the first quark plus that of the gluons emitted on the "open" side of the lines in Figs. 1(b) and 1(c). These propagators obey the following equations:

$$q^2\frac{d}{dq^2}H_g^i(q^2;x)=V_g(q^2)H_g^i(q^2;x)+\int_x^1\frac{dz}{z}\frac{\alpha(z(1-z)q^2)}{4\pi}\sum_j\frac{\hat{P}_g^{q\bar{q}}(z)}{N_f}H_g^i\left[\lambda(z)q^2;\frac{x}{z}\right]$$
$$+\int_x^1\frac{dz}{z}\frac{\alpha(z(1-z)q^2)}{4\pi}\hat{P}_g^{gg}(z)H_g^i\left[\lambda(z)q^2;\frac{x}{z}\right]$$
$$+\int_0^x\frac{dz}{1-z}\frac{\alpha(z(1-z)q^2)}{4\pi}\hat{P}_g^{gg}(z)\sigma_g(\lambda(z)q^2,Q_0^2)H_g^i\left[\lambda(1-z)q^2;\frac{x-z}{1-z}\right], \tag{2.1a}$$

$$q^2\frac{d}{dq^2}H_j^i(q^2;x)=V_q(q^2)H_j^i(q^2;x)+\int_x^1\frac{dz}{z}\frac{\alpha(z(1-z)q^2)}{2\pi}\hat{P}_q^{gq}(z)H_g^i(\lambda(z)q^2;x/z)$$
$$+\int_x^1\frac{dz}{z}\frac{\alpha(z(1-z)q^2)}{2\pi}\hat{P}_q^{gq}(z)\sigma_g(\lambda(z)q^2,Q_0^2)H_j^i\left[\lambda(1-z)q^2;\frac{x-z}{1-z}\right], \tag{2.1b}$$

and

$$q^2\frac{d}{dq^2}\sigma_g(q^2,Q_0^2)=\sigma_g(q^2,Q_0^2)V_g(q^2)+\tfrac{1}{2}\int dz\frac{\alpha(z(1-z)q^2)}{2\pi}\hat{P}_g^{gg}(z)\sigma_g(\lambda(z)q^2,Q_0^2)\sigma_g(\lambda(1-z)q^2,Q_0^2), \tag{2.1c}$$

where $V_g(q^2)$ and $V_q(q^2)$ are virtual potentials given by

$$V_q(q^2)=-\int_\epsilon^{1-\epsilon}dz\frac{\alpha(z(1-z)q^2)}{2\pi}[\tfrac{1}{2}\hat{P}_g^{gg}(z)+\hat{P}_g^{q\bar{q}}(z)], \tag{2.2a}$$

$$V_g(q^2)=-\int_\epsilon^{1-\epsilon}dz\frac{\alpha(z(1-z)q^2)}{2\pi}[\tfrac{1}{2}\hat{P}_q^{qg}(z)+\tfrac{1}{2}\hat{P}_q^{gq}(z)]. \tag{2.2b}$$

σ_g is the probability that gluons do not produce $q\bar{q}$ pairs.

The CJ equations have the convenient graphical representation shown in Figs. 2(a) and 2(b). Equation (2.1c) for σ_g can be rewritten as [see Fig. 2(c)]

$$\frac{d\sigma}{d\tau}=-\sigma\left[\frac{C_A}{b\pi}\int_{\tau_0}^{\tau}\frac{d\tau'}{\tau'}[1-\sigma(\tau')]-\frac{11C_A}{12\pi}\alpha(\tau)(1-\sigma)+\frac{N_f}{6\pi}\alpha(\tau)\right] \tag{2.3}$$

with

$$\tau=\ln(q^2/\Lambda^2),\quad \tau_0=\ln(Q_0^2/\Lambda^2),\quad \alpha(\tau)=\frac{1}{b\tau},\quad b=\frac{11N_C-2N_f}{12\pi}.$$

This is the same as JM and Amati *et al.*[10] The color-singlet distribution is given by (see Fig. 3)

$$\frac{1}{\sigma_\alpha}\frac{d\sigma_\alpha}{dx_1dx_2}\bigg|_{\rm CS}=\sum_{\beta\gamma\delta}{}'\int_{Q_0^2}^{Q^2}\frac{dk^2}{k^2}\int_{x_1+x_2}^1\frac{dx}{x^2}D_\alpha^\beta(Q^2,k^2;x)\int_{x_1/x}^{1-x_2/x}\frac{dz}{z(1-z)}\frac{\alpha(z(1-z)k^2)}{2\pi}\hat{P}_\beta^{\gamma\delta}(z)H_\gamma^{q_l}\left[\lambda(z)k^2;\frac{x_1}{xz}\right]$$
$$\times H_\delta^{\bar{q}_m}\left[\lambda(1-z)k^2;\frac{x_2}{x(1-z)}\right], \tag{2.4}$$

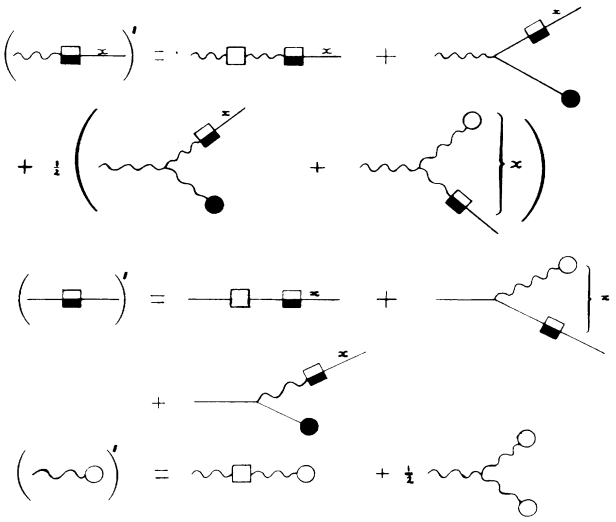

FIG. 2. Graphical depiction of Eqs. (2.1)—(2.3).

where $x=x_1+x_2$ is the momentum carried away by the entire cluster including the gluons and α refers to quark or gluon. Equations (2.1)—(2.4) are integrated from Q_0^2 to Q^2. The solution of these equations is discussed by JM.

III. MODIFICATION OF JET CALCULUS TO ACCOMMODATE ANGULAR ORDERING

A. Coherence effects in gluon emission

Recently, it has been found[11–13] that, in addition to collinear mass singularities, there are soft perturbative singularities associated with the emission of low-energy gluons. These effects have been carefully studied by a number of workers. To describe these effects, we follow the treatment of Mueller.[11] (See also Ref. 12.)

We recall that in the LLA only ladder diagrams are required [see Fig. 4(a)]. Their contribution has the generic form[3,11]

$$\sum_{n=1}^{\infty}\frac{1}{n!}\left[\frac{C_A\alpha_s}{\pi}\right]^n \ln^n\left[\frac{Q^2}{Q_0^2}\right]\frac{\ln^{n-1}(1/x)}{(n-1)!} \tag{3.1}$$

while the diagrams with crossed rungs contribute

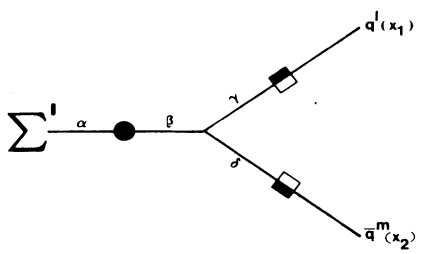

FIG. 3. Graphical representation of Eq. (2.4).

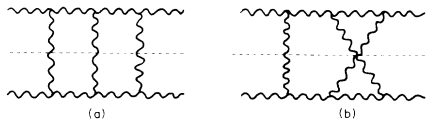

FIG. 4. (a) Ladder diagram of order α_s^3. (b) A crossed diagram of the same order.

$$\sum_{n=1}^{\infty}\frac{1}{n!}\left[\frac{C_A\alpha_s}{\pi}\right]^n \ln^{n-1}\left[\frac{Q^2}{Q_0^2}\right]\frac{\ln^n(1/x)}{(n-1)!}\ . \tag{3.2}$$

We see from above that crossed rungs can contribute substantially in the low-x region.

For example, in order α_s^3, the ladder diagram of Fig. 4(a) contributes

$$\ln^2\left[\frac{Q^2}{Q_0^2}\right]\ln\frac{1}{x}-3\ln\left[\frac{Q^2}{Q_0^2}\right]\ln^2\frac{1}{x}+2\ln^3\frac{1}{x} \tag{3.3}$$

while the crossed diagram [Fig. 4(b)] gives

$$-\ln\left[\frac{Q^2}{Q_0^2}\right]\ln^2\frac{1}{x}+2\ln^3\frac{1}{x}\ . \tag{3.4}$$

Their sum is

$$\ln^2\left[x^2\frac{Q^2}{Q_0^2}\right]\ln\frac{1}{x}\ . \tag{3.5}$$

Thus the addition of the crossed diagram changes the $\ln^2(Q^2/Q_0^2)$ of LLA to $\ln^2(x^2Q^2/Q_0^2)$. Mueller[11] has shown that this form can still be interpreted in terms of the semiclassical, probabilistic language of ladder diagrams, provided we order the emission angles in subsequent branchings.

Let us consider the branching indicated in Fig. 5. We define the angular variable

$$\xi=\frac{q_1\cdot q_2}{\omega_1\omega_2}$$

$$\simeq 1-\cos\theta_{12}\ \ (\text{if } q_i^2\simeq 0)\ . \tag{3.6}$$

The effect of interference of soft gluons is taken into account to leading order by requiring

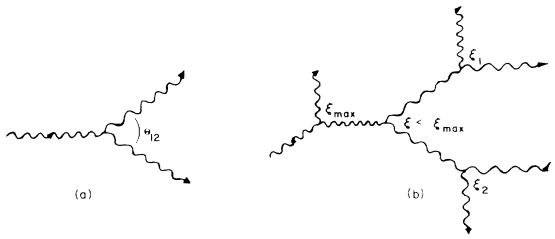

FIG. 5. (a) The basic branching process: gluon→gluon + gluon. (b) Ordering angular variables in subsequent branchings according to Eq. (3.7).

$$\xi_1,\xi_2<\xi<\xi_{\max}\le 1\ , \tag{3.7}$$

where ξ_1 and ξ_2 are the angular variables of the eventual branchings of gluons 1 and 2, while $\xi_{\max}$ is the angular variable of the vertex at which the incoming gluon was produced. Its virtuality is given by

$$\begin{aligned} q^2&=q_1{}^2+q_2{}^2+2q_1\cdot q_2\\ &=q_1{}^2+q_2{}^2+2\omega_1\omega_2\xi\ . \end{aligned} \tag{3.8}$$

When all the energies are of the same order, we see that ordering of ξ is equivalent to ordering of virtuality.

When we write the jet-calculus equations, we keep the convention that what appears at each vertex is $\alpha(p_t{}^2)$. This is based on the physics of the situation, and is the same convention implemented by MW in their Monte Carlo calculations. The effect of Mueller's discovery is to change the independent variable in the equations. Let us examine the kinematics of a typical decay vertex to see how this is to be implemented.

Consider a parton with virtuality q^2 and energy ω which decays into partons of virtuality $q_1{}^2$ and energy $z\omega$, and $q_2{}^2$, $(1-z)\omega$. Because of the basic relation

$$q^2=\frac{q_1{}^2+p_t{}^2}{z}+\frac{q_2{}^2+p_t{}^2}{1-z}\ , \tag{3.9}$$

we expect that $p_t{}^2=z(1-z)q^2$ for z near the ends of the allowed range.

However, near these points q^2 is no longer the appropriate variable for the differential equations, because the strong ordering is not in q^2. Rather, we need to write

$$\begin{aligned} q^2&=q_1{}^2+q_2{}^2+2q_1\cdot q_2\\ &=q_1{}^2+q_2{}^2+2z(1-z)\omega^2\xi\ , \end{aligned} \tag{3.10}$$

where $\xi=1-\cos(\theta_{12})$ is strongly ordered. We use p^2 as the variable for the integrodifferential equations, where

$$2\omega^2\xi=p^2\ . \tag{3.11}$$

This is strongly ordered also and has the same dimensions as q^2.

This means that the vertex in the differential equation is represented by $\alpha(z^2(1-z)^2p^2)$. Thus we are led to replace integrals such as

$$\int_{Q_0{}^2/Q^2}^1\frac{dz}{z}\alpha(z(1-z)q^2) \tag{3.12}$$

of Refs. 9 and 10 by (see Appendix A)

$$\int_{Q_0/P}^1\frac{dz}{z}\alpha(z^2(1-z)^2p^2)\ . \tag{3.13}$$

(See also Kiselev.[15]) In addition, we use this replacement inside the propagators in the CJ equations to translate them into the variable p^2.

We thereby obtain equations in the variable p^2 which are similar to our previous equations and can be solved in a similar way. However, before we compare with the previous results, we must translate our results back into q^2. As is clear from Eqs. (3.10) and (3.11) above, to obtain a given q^2 we must consider a *range* of p^2, and these p^2 values are (much) higher than q^2. We will achieve the comparison by averaging over appropriate p^2, as explained in Sec. IV below.

Our averaging procedure plays a role similar to a particular step in MW's Monte Carlo model—the step in which the q^2 for the two-jet event is reconstructed and the event is discarded if this mass falls outside the given range. In both calculations the use of strong ordering in a parameter which is not the virtuality requires ultimately a reconciliation with the physical necessity of using the invariant mass as a specification for the system. This introduces some inefficiency into both procedures.

Note that the energy fraction z could also be interpreted as a light-cone parameter without changing much. This fraction is then invariant under Lorentz boosts along the jet axis. We thus see that the scheme is basically Lorentz invariant (under longitudinal boosts) in spite of its use of the angular variable ξ. Hence we expect the results to be Lorentz invariant, as MW have shown empirically.

B. Modified CJ equations

In the CJ equations we make the above replacements to obtain

$$\begin{aligned} p^2\frac{d}{dp^2}\tilde{H}_g^i(p^2;x)=\tilde{V}_g(p^2)\tilde{H}_g^i(p^2;x)&+\int_x^1\frac{dz}{z}\frac{\alpha(z^2(1-z)^2p^2)}{2\pi}\sum_j\frac{\hat{P}_g^{q\bar{q}}(z)}{N_f}\tilde{H}_j^i\left[\lambda(z^2)p^2;\frac{x}{z}\right]\\ &+\int_x^1\frac{dz}{z}\frac{\alpha(z^2(1-z)^2p^2)}{4\pi}\hat{P}_g^{gg}(z)\tilde{H}_g^i\left[\lambda(z^2)p^2;\frac{x}{z}\right]\\ &+\int_0^x\frac{dz}{1-z}\frac{\alpha(z^2(1-z)^2p^2)}{4\pi}\hat{P}_g^{gg}(z)\tilde{\sigma}_g(\lambda(z^2)p^2,Q_0{}^2)\tilde{H}_g^i\left[\lambda((1-z)^2)p^2;\frac{x-z}{1-z}\right], \end{aligned} \tag{3.14a}$$

$$\begin{aligned} p^2\frac{d}{dp^2}\tilde{H}_j^i(p^2;x)=\tilde{V}_q(p^2)\tilde{H}_j^i(p^2;x)&+\int_x^1\frac{dz}{z}\frac{\alpha(z^2(1-z)^2p^2)}{2\pi}\hat{P}_q^{gq}(z)\tilde{H}_g^i\left[\lambda(z^2)p^2;\frac{x}{z}\right]\\ &+\int_x^1\frac{dz}{z}\frac{\alpha(z^2(1-z)^2p^2)}{2\pi}\hat{P}_q^{gq}(z)\tilde{\sigma}_g(\lambda(z^2)p^2,Q_0{}^2)\tilde{H}_j^i\left[\lambda((1-z)^2)p^2;\frac{x-z}{1-z}\right], \end{aligned} \tag{3.14b}$$

and

$$p^2\frac{d}{dp^2}\tilde{\sigma}_g(p^2,Q_0^2)=\tilde{\sigma}_g(p^2,Q_0^2)\tilde{V}_g(p^2)+\tfrac{1}{2}\int dz\frac{\alpha(z^2(1-z)^2p^2)}{2\pi}\hat{P}_g^{gg}(z)\tilde{\sigma}_g(\lambda(z^2)p^2,Q_0^2)\tilde{\sigma}_g[\lambda((1-z)^2)p^2,Q_0^2]\ . \quad (3.14c)$$

Note that corresponding changes should be made in the virtual potentials as well (Fig. 1). The colorless-cluster [color-singlet (CS)] distributions take the form

$$\frac{1}{\tilde{\sigma}_\alpha}\frac{d\tilde{\sigma}_\alpha}{dx_1dx_2}\bigg|_{\rm CS}=\sum_{\beta\gamma\delta}{}'\int_{Q_0^2}^{P}\frac{dk^2}{k^2}\int_{x_1+x_2}^{1}\frac{dx}{x^2}D_\alpha^\beta(P^2,k^2,x)$$
$$\times\int_{x_1/x}^{1-x_2/x}\frac{dz}{z(1-z)}\frac{\alpha(z^2(1-z)^2k^2)}{2\pi}\hat{P}_\beta^{\gamma\delta}(z)\tilde{H}_\gamma^{q_l}\left[\lambda(z^2)k^2;\frac{x_1}{xz}\right]$$
$$\times\tilde{H}_\delta^{\bar{q}_m}\left[\lambda((1-z)^2)k^2;\frac{x_2}{x(1-z)}\right]\ . \quad (3.15)$$

As we demonstrated in Refs. 8 and 9, Eqs. (3.14) and (3.15) may be converted into a set of coupled ordinary differential equations in moment space. These have the feature that the nth moment of $\tilde{H}$ depends on the $n-1$ and all lower moments, including $\tilde{\sigma}$. The normalization of the quantities is completely determined by the initial conditions at $P^2=Q_0^2$ (see Ref. 9). Obviously from (3.15), the moments of colorless-cluster distributions depend on special gauge-invariant combinations of $\tilde{H}$ and $\tilde{\sigma}$.

The new coherent equations differ from those in the appendixes of Ref. 9 in that the quantities $\Sigma(k^2)$ and $\Xi(k^2)$ defined there by

$$\Sigma(k^2)=\frac{1}{\pi}\int_{Q_0^2}^{k^2}\frac{dk'^2}{k'^2}\alpha(k'^2)[1-\sigma_g(k'^2)]\ ,$$
$$\Xi(k^2)=\int_{Q_0^2}^{k^2}\frac{dk'^2}{k'^2}\alpha(k'^2)\sigma_g(k'^2) \quad (3.16)$$

are replaced by $\frac{1}{2}\tilde{\Sigma}(p^2)$ and $\frac{1}{2}\tilde{\Xi}(p^2)$, respectively. A standard differential-equation package such as RKF45 was used to simultaneously integrate the equations from Q_0^2 to P^2 for $\tilde{\sigma}_g$, the propagators and the CS distributions.

The results obtained by the solution of these equations are in moment space. We solve for eight moments. These are inverted to give propagators and CS distributions in x. To achieve this, we use the conventional method due to Yndurain[16] and also the Legendre expansion as advocated by Jones and Opsahl.[17] The need for the latter arises because Yndurain's technique cannot be extended to $x<0.2$ if one has 8 moments available. Also Yndurain's method tends to overestimate the functional value for x values lower than 0.3.

IV. A RECONSTRUCTION SCHEME AND ITS DEPENDENCE ON KINEMATICAL BOUNDS

The solutions of Eqs. (3.14)—(3.16) are functions of P^2 and Q_0^2. They cannot, however, be compared to the JM results directly [see Eqs. (2.1)] because the two formalisms use different evolution variables as discussed above and in Appendix A. To establish a comparison between the incoherent and coherent approaches, in the absence of a unique and rigorous analytical procedure, we have devised a "reconstruction" (or averaging) scheme. Two versions of this scheme are discussed in Secs. IV A—IV C below. Their impact on the results is discussed in Secs. IV D and V.

A. A simple method of reconstruction

This method (A) is based on the (asymptotically correct) relationship

$$z^2(1-z)^2P^2=z(1-z)Q^2\ , \quad (4.1)$$

where Q^2 and P^2 are the variables in the incoherent and coherent branching schemes. For a fixed Q^2, we have

$$(P^2)_{\rm min}=\frac{Q^2}{[z(1-z)]_{\rm max}}=4Q^2 \quad (4.2a)$$

$$(P^2)_{\rm max}=\frac{Q^2}{Q_0^2/Q^2}=\frac{Q^4}{Q_0^2}\ . \quad (4.2b)$$

Thus given a function $\tilde{f}(P^2,n)$, which can be $\tilde{\sigma}_g$, a propagator or a CS distribution, we can define the "reconstructed" or averaged quantity $\bar{f}(Q^2,n)$ using the mean-value theorem for integrals:

$$\bar{f}_A(Q^2,n)=\frac{1}{Q^4/Q_0^2-4Q^2}I_A(Q^2,n)\ , \quad (4.3)$$

where

$$I_A(Q^2,n)=\int_{4Q^2}^{Q^4/Q_0^2}\tilde{f}(P^2,n)dP^2\ .$$

Note that the subscript A refers to this first technique of averaging. The approximations used here are similar to those used in all our differential equations. We expect the results to be approximately correct at large Q^2; and since in that case the region of integration for P^2 covers only large P^2, we should not lose much accuracy by neglect of the nonasymptotic terms.

B. A refined method

Before discussing the evaluation of $\bar{f}_A$, we first take a closer look at the kinematics involved. From Eq. (3.10) we see that the behavior near $z=0$ or $(1-z)=0$ is influenced by the nonasymptotic terms q_1^2 and q_2^2. Consider, for instance, the original branching of the virtual photon of mass Q (e.g., in e^+e^- annihilation) into two partons of

masses Q_1 and Q_2. In the rest frame of the photon their four-momenta are

$$\begin{aligned} Q^\mu &= (Q,0,0,0) , \\ P_1^\mu &= (E_1, q\sin\theta, 0, q\cos\theta) , \\ P_2^\mu &= (E_2, -q\sin\theta, 0, -q\cos\theta) , \end{aligned} \tag{4.4}$$

where $q = |\mathbf{q}|$ and θ is the angle subtended by $\mathbf{q}$ and the z axis ($0 \le \theta \le \pi/2$). The process takes place in the xz plane.

The following relationships are obvious:

$$\begin{aligned} E_1 &= \frac{1}{2Q}(Q^2 + {Q_1}^2 - {Q_2}^2) , \\ E_2 &= \frac{1}{2Q}(Q^2 - {Q_1}^2 + {Q_2}^2) , \\ q^2 &= \frac{1}{4Q^2}[Q^2 - (Q_1+Q_2)^2][Q^2 - (Q_1-Q_2)^2] . \end{aligned} \tag{4.5}$$

As in MW, we next boost the momenta along the z axis. This gives

$$\begin{aligned} Q'^\mu &= M(\gamma) Q^\mu , \\ P'^\mu_1 &= M(\gamma) P_1^\mu , \\ P'^\mu_2 &= M(\gamma) P_2^\mu , \end{aligned} \tag{4.6}$$

where

$$M(\gamma) = \begin{bmatrix} \cosh\gamma & \sinh\gamma \\ \sinh\gamma & \cosh\gamma \end{bmatrix} .$$

Then, from $\mathbf{P}'_1 \cdot \mathbf{P}'_2 = 0$ (when $\theta_{12} = \pi/2$), Eq. (4.6) yields

$$(E_1E_2 - q^2\cos^2\theta)\cosh^2\gamma + (E_2 - E_1) q\cos\theta \sinh\gamma \cosh\gamma - (E_1E_2 + q^2\sin^2\theta) = 0 . \tag{4.7}$$

For simplicity, we can assume $E_1 = E_2 = E$, so that $Q = 2E$, and Eq. (4.7) admits the solution

$$\cosh^2\gamma = \frac{Q^2/4 + q^2\sin^2\theta}{Q^2/4 - q^2\cos^2\theta} \tag{4.8}$$

with

$$q^2 = \frac{Q^2}{4} - {Q_1}^2 .$$

Equation (4.8) reaches a maximum and a minimum for $\theta = 0$ and $\pi/2$, respectively. We can then obtain the bounds on the variable $P^2 = 2\omega^2\xi$ in Eq. (3.11) as follows: when $\theta_{12} = \pi/2$, and with $\omega^2 = Q^2\cosh^2\gamma$ [from Eq. (4.6)], P^2 becomes

$$P^2 = 2Q^2\cosh^2\gamma .$$

Thus using Eq. (4.8), we obtain the inequality

$$4Q^2 - 8{Q_1}^2 \le P^2 \le \frac{1}{2}\frac{Q^4}{{Q_1}^2} . \tag{4.9}$$

When the mass Q_1 is small, i.e., $Q_1 \sim Q_0$, Eq. (4.9) can be approximated as

$$4Q^2 \le P^2 \le \frac{1}{2}\frac{Q^4}{{Q_0}^2} . \tag{4.10}$$

This inequality forms the basis of our second reconstruction technique (hereafter referred to as *B*). Comparison of (4.10) and (4.2) shows that the two methods differ only in a factor of 2 in the upper limit. In analogy with Eq. (4.3) we now define

$$\bar{f}_B(Q^2,n) = \frac{1}{\frac{1}{2}\frac{Q^4}{{Q_0}^2} - 4Q^2} I_B(Q^2,n) , \tag{4.11}$$

where

$$I_B(Q^2,n) = \int_{4Q^2}^{Q^4/2{Q_0}^2} \tilde{f}(P^2,n) dP^2 .$$

We now consider the crucial question of how I_A and I_B can be most accurately evaluated.

C. Evaluation of I_A and I_B

We have found a trick which enables these averages to be evaluated at the same time as the $\tilde{\sigma}$, $\tilde{H}$, etc. by enlarging the system of differential equations. To be specific we consider the second averaging procedure, i.e., Eq. (4.11). Defining $p = P/\Lambda$, $q = Q/\Lambda$, we can write

$$I(Q^2,n) = \Lambda^2 J(q^2) . \tag{4.12}$$

Taking the derivative with respect to q^2 and suppressing the n dependence for simplicity, we get

$$q^2\frac{dJ(q^2)}{dq^2} = \frac{q^4}{{q_0}^2}\tilde{f}\left(\frac{q^4}{2{q_0}^2}\right) - 4q^2\tilde{f}(4q^2) . \tag{4.13}$$

If we let

$$u = \frac{q^4}{2{q_0}^2}, \quad v = 4q^2 \tag{4.14}$$

and

$$h_1(q^2) = \tilde{f}(q^4/2{q_0}^2), \quad h_2(q^2) = \tilde{f}(4q^2) , \tag{4.15}$$

Eq. (4.13) gives

$$q^2\frac{dJ(q^2)}{dq^2} = 2uh_1(q^2) - vh_2(q^2) . \tag{4.16}$$

For the case of the propagators the solution of (4.16) is fairly straightforward. The propagators in moment space obey equations of the form

$$\kappa^2\frac{d\tilde{f}(\kappa^2)}{d\kappa^2} = g(\kappa^2) , \tag{4.17}$$

where the functions $g(\kappa^2)$ are written explicitly in JM (Appendix A). In turn, the functions $h_1(q^2)$ and $h_2(q^2)$ satisfy differential equations obtained by differentiating Eqs. (4.15a) and (4.15b) with respect to q^2 and combining with Eq. (4.17) to give

$$q^2\frac{dh_1(q^2)}{dq^2} = 2g(u) , \tag{4.18}$$

$$q^2\frac{dh_2(q^2)}{dq^2}=g(v)\ . \tag{4.19}$$

Equations (4.18), (4.19), and (4.16) are solved simultaneously subject to the initial conditions specified at $Q^2=8Q_0{}^2$: namely, $I(8Q_0{}^2)=0$ from Eq. (4.12).

The above procedure, as it stands is not directly applicable to the colorless-cluster distributions. Some major modifications are needed in the differential equations for $\tilde{f}(u)$ and $\tilde{f}(v)$. From JM Appendix A, Eq. (A3)] we know that the CC distributions in moment space are given by equations of the form [see Eq. (3.15)]

$$\tilde{f}_\alpha(P^2,n)=\sum_{\beta\gamma\delta}{}'\int_{Q_0{}^2}^{P^2}\frac{dk^2}{k^2}D_\alpha^\beta(P^2,k^2,n)Z_\beta(k^2,n)\ , \tag{4.20}$$

where $Z_\beta(k^2)$ is a lengthy expression involving propagators and Altarelli-Parisi P functions in moment space, and the subscript α specifies the type of jet. Taking the derivative with respect to ln (P^2) produces an extra term owing to the P^2 dependence of D_α^β:

$$\frac{\partial}{\partial\ln P^2}\tilde{f}_\alpha(P^2,n)=\sum_{\beta\gamma\delta}{}'D_\alpha^\beta(P^2,P^2,n)Z_\beta(P^2,n)+\sum_{\beta\gamma\delta}{}'\int_{Q_0{}^2}^{P^2}\frac{dk^2}{k^2}\left[\frac{\partial}{\partial\ln P^2}D_\alpha^\beta(P^2,k^2,n)\right]Z_\beta(k^2,n)\ . \tag{4.21}$$

In the first term, we substitute $D_\alpha^\beta(P^2,P^2)=\delta_\alpha^\beta$, and we simplify the second one through the Altarelli-Parisi equations to obtain

$$\frac{\partial}{\partial\ln P^2}\tilde{f}_\alpha(P^2,n)=Z_\alpha(P^2,n)+\sum_{\beta\gamma\delta}{}'\sum_\epsilon\frac{\alpha(P^2)}{2\pi}\int_{Q_0{}^2}^{P^2}\frac{dk^2}{k^2}A_{\epsilon\alpha}^n D_\epsilon^\beta(P^2,k^2,n)Z_\beta(k^2,n)\ . \tag{4.22}$$

Equation (4.22) simplifies further by making use of Eq. (4.20):

$$\frac{\partial}{\partial\ln P^2}\tilde{f}_\alpha(P^2,n)=Z_\alpha(P^2,n)+\frac{\alpha(P^2)}{2\pi}\sum_\epsilon A_{\epsilon\alpha}^n\tilde{f}_\epsilon(P^2,n)\ . \tag{4.23}$$

This equation implies mixing between quark and gluon jets, since for a given α, ϵ takes on both quark and gluonic values.

For the specific cases of gluon jets ($\alpha=g$) and quark jets ($\alpha=q$), this yields

$$P^2\frac{\partial}{\partial P^2}\tilde{f}_g(P^2,n)=\tfrac{1}{2}G(P^2,n)+\frac{\alpha(P^2)}{2\pi}[2N_f A_{qg}^n\tilde{f}_q(P^2,n)+A_{gg}^n\tilde{f}_g(P^2,n)]\ , \tag{4.24}$$

$$P^2\frac{\partial}{\partial P^2}\tilde{f}_q(P^2,n)=Q(P^2,n)+\frac{\alpha(P^2)}{2\pi}[A_{qq}^n\tilde{f}_q(P^2,n)+A_{gq}^n\tilde{f}_g(P^2,n)]\ . \tag{4.25}$$

In Eqs. (4.24) and (4.25) the notation of JM [Appendix A, Eq. (A3)] for the functions G and Q has been used. Based on these two equations, results analogous to (4.18) and (4.19) are easily derived for the colorless clusters. The differential equations in reconstruction scheme A can be set up in exactly the same way.

The solution of these equations for propagators and colorless clusters is achieved by the routine RKF45, which provides a very rapid solution for the large number of coupled differential equations (132 in our case, with eight moments) needed to obtain all the moments and averages. The accuracy of the solution is evidenced by the quark and gluon momentum-conservation sum rules[8,9] obeyed by the averaged quantities:

$$\left\langle\int_0^1\frac{1}{\sigma}\frac{d\sigma}{dx}\right|_{\rm CS}x\,dx\right\rangle=1-\sum_i\bar{H}_j^i(Q^2,1)\ \text{ for quarks}\ , \tag{4.26}$$

$$\left\langle\int_0^1\frac{1}{\sigma}\frac{d\sigma}{dx}\right|_{\rm CS}x\,dx\right\rangle=1-\bar{\sigma}-2\sum_i\bar{H}_g^i(Q^2,1)\ \text{for gluons}\ . \tag{4.27}$$

Typically, our solution obeys the sum rules to one part in 10^{10}.

It is to be noted that the direct evaluation of I_A and I_B is also possible through the use of standard routines such as DO1GAF from NAGLIB. This procedure, however, is lacking in numerical accuracy relative to the above method (the sum rules are obeyed to 1 part in 10^7), in addition to being less elegant and much more time consuming. Also the Q^2 dependence of $\bar{f}_{A,B}$ and $I_{A,B}$ is not at all transparent. We have used this direct evaluation as a check of our differential-equation calculations.[18]

D. Example: σ_g, the probability that gluons only produce gluons

To make our procedure clear, we describe here the computations for the probability σ_g that gluons do not produce quark-antiquark pairs. This is a good quantity to examine in detail because there is an integrodifferential equation which involves σ_g and nothing else, so analytic tools can be applied easily to check the computations.

The equation for σ_g is represented graphically in Fig. 2. After some manipulation, Eqs. (2.1c) and (3.14c) take the form

$$\frac{d\sigma}{d\tau}=-\sigma\left[\frac{C_A}{\pi b}d\int_{\tau_0}^{\tau}\frac{d\tau'}{\tau'}[1-\sigma(\tau')]-\frac{11C_A}{12\pi}\alpha(\tau)(1-\sigma)+\frac{N_f}{6\pi}\alpha(\tau)\right], \tag{4.28}$$

where $d=1$ for the conventional (JM) case, and $d=\frac{1}{2}$ for the modified CJ equation. This equation has the asymptotic solution

$$\sigma_g(\tau)=\left[\frac{\tau_0}{\tau}\right]^{d(C_A/\pi b)\tau}\left[\frac{Q^2}{Q_0^2}\right]^{d(C_A/\pi b)}. \tag{4.29}$$

Clearly the old and new σ_g are asymptotically related by

$$[\sigma_g(\tau)]_{\text{modified CJ}}=[\sigma_g(\tau)_{\text{JM}}]^{1/2}. \tag{4.30}$$

This is similar to the behavior of the Sudakov form factor seen by MW (Ref. 13). In Fig. 6 the results for the solution of Eq. (4.28) are displayed[19] for both values of d: we see that the change of exponent in (4.29) has drastic consequences; the variation in P^2 is much slower than that in Q^2. It is important to note that a similar change occurs in the propagators when we go from the Q^2 to the P^2 formalisms, although for simplicity these curves are not plotted here.

Now we average over the appropriate range of P^2 using methods A and B described earlier. These results are also shown in Fig. 6, labeled A and B. We see that initially the reconstructed solutions drop a little more rapidly than the JM solution; at large values of Q^2, $\bar{\sigma}_A$ differs from σ_{JM} by about a factor of 4 and $\bar{\sigma}_B$ by a factor of about 2. A possible interpretation of the damping is that the phase-space limitation due to the angular ordering inhibits gluons going into gluons. (The $g\to gg$ probability function peaks strongly at low z. Thus change of the same range of integration in z cuts out much more $g\to gg$ than it does of the flatter $g\to q\bar{q}$.)

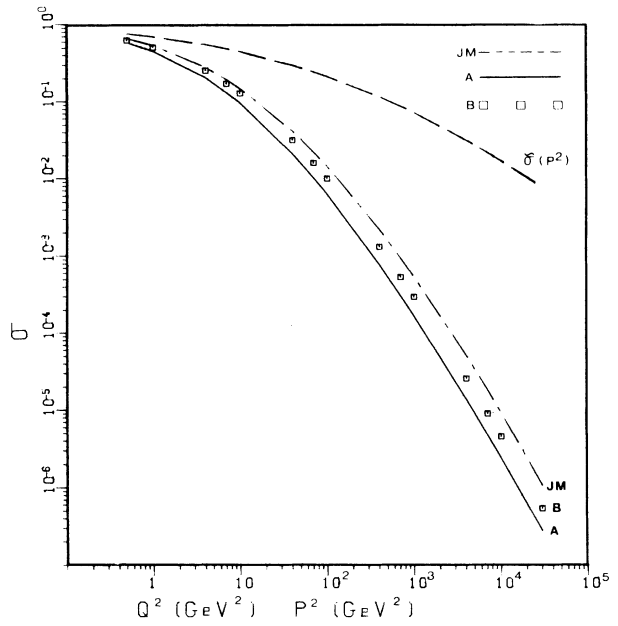

FIG. 6. σ_g as a function of Q^2 (at $Q_0^2=0.062$ GeV^2) for σ_{JM} and reconstructed $\bar{\sigma}_A$ and $\bar{\sigma}_B$ functions, and as a function of P^2 for the intermediate stage $\tilde{\sigma}$.

Comparison of $\bar{\sigma}_A$ and $\bar{\sigma}_B$ shows that the results are not very different. In fact

$$\bar{\sigma}_A<\bar{\sigma}_B<2\bar{\sigma}_A. \tag{4.31}$$

To see this, we define the positive difference

$$\Delta_{AB}=I_A-I_B=\int_{Q^4/2Q_0^2}^{Q^4/Q_0^2}\tilde{\sigma}(P^2)dP^2. \tag{4.32}$$

Then

$$\bar{\sigma}_A\approx\frac{I_A}{Q^4/Q_0^2} \tag{4.33}$$

and

$$\bar{\sigma}_B\approx\frac{I_B}{Q^4/2Q_0^2}=2\bar{\sigma}_A-\frac{\Delta_{AB}}{Q^4/2Q_0^2} \tag{4.34}$$

or

$$R\equiv\frac{\bar{\sigma}_B}{\bar{\sigma}_A}=2-\frac{\Delta_{AB}}{(Q^4/2Q_0^2)\bar{\sigma}_A}\to 2 \text{ as } Q^2\to\infty \tag{4.35}$$

because $\tilde{\sigma}(P^2)$ drops off fairly rapidly as $P^2\to\infty$. The results of our calculations for this ratio as a function of Q^2 are shown in Table I.

We shall see in Sec. V that, when methods A and B are applied to other quantities of interest, which drop more slowly with P^2 than σ_g, the corresponding ratio is even smaller. For instance, for the propagators the results of the two schemes differ by less than a factor of 1.6; for all the physical quantities (colorless cluster distributions) schemes A and B differ by less than 7%.

Another property of interest is the Q_0^2 dependence of σ_g, shown in Fig. 7. The effect of increasing Q_0^2 is to increase σ_g, in both the JM and reconstructed schemes: we only present the results of method A for comparison.

TABLE I. Q^2 dependence of the ratio R, defined in Eq. (4.35).

Q^2 (GeV^2)	R
100	1.584
1000	1.777
4000	1.859
10000	1.902
30000	1.939

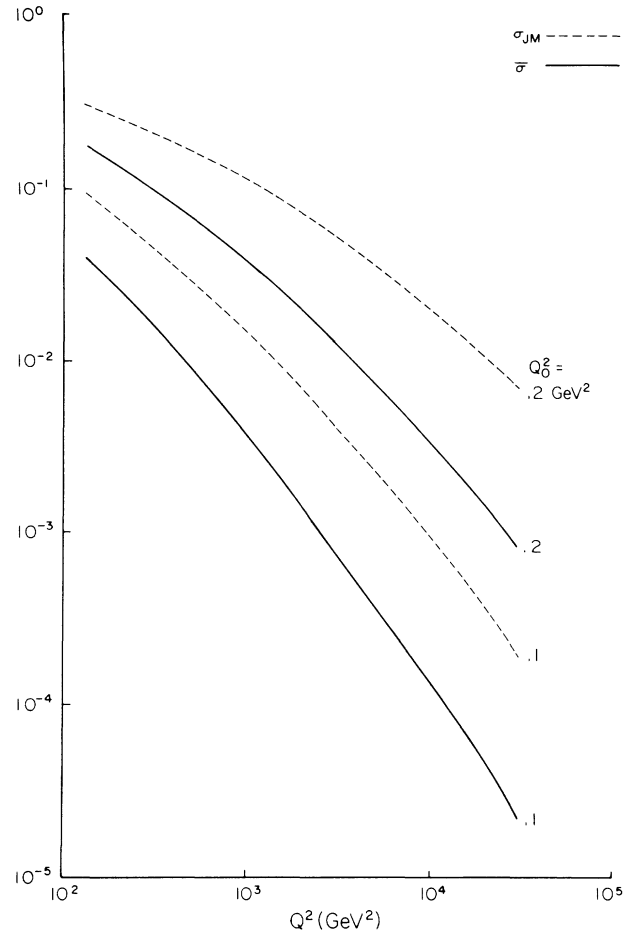

FIG. 7. Behavior of σ_g and $\bar{\sigma}_A$ at various Q_0^2 as a function of Q^2.

Since Q_0^2 is a measure of the mass of the colorless clusters, we can interpret this as the suppression of the $g \to q\bar{q}$ channel as Q_0 increases. Note that, as expected on physical grounds, σ_g reaches its highest value ($=1$) at the boundary. The Q_0^2 variation of the other quantities, i.e., propagators and colorless cluster distributions, follows a similar trend to that exhibited by σ_g, and thus will not be shown.

Returning to Fig. 6, possibly the most remarkable aspect of our result is that, after the reconstruction has been carried out, the probability σ_g changes so little. As we will see, this is also true of the propagators and colorless-cluster distributions discussed below. This is, of course what we expect—the angular ordering condition could not completely change the results. It is satisfying to discover that the computed solutions have this property, despite the very different looking values in the intermediate (P^2) step.

V. RESULTS

In this section we make a comparison between at least one version of the reconstructed results (the results of method B are not shown in all cases) and the conventional JM results; comparison with the work of Marchesini-Webber[13] is made when applicable. We have set $\Lambda = 0.2$ GeV and $Q_0^2 = 0.062$ GeV^2 unless otherwise stated.

A. Moments

As mentioned earlier, the coupled system of Eqs. (3.14) and (3.15) is solved in moment space. Eight moments are used.[17] The outputs $\tilde{H}_j^i(P^2,n)$, etc., are then averaged to obtain the reconstructed $\bar{H}_j^i(Q^2,n)$ using the method given in Sec. IV C.

The results for the quark (favored and unfavored) and gluon propagator moments are shown in Figs. 8–11

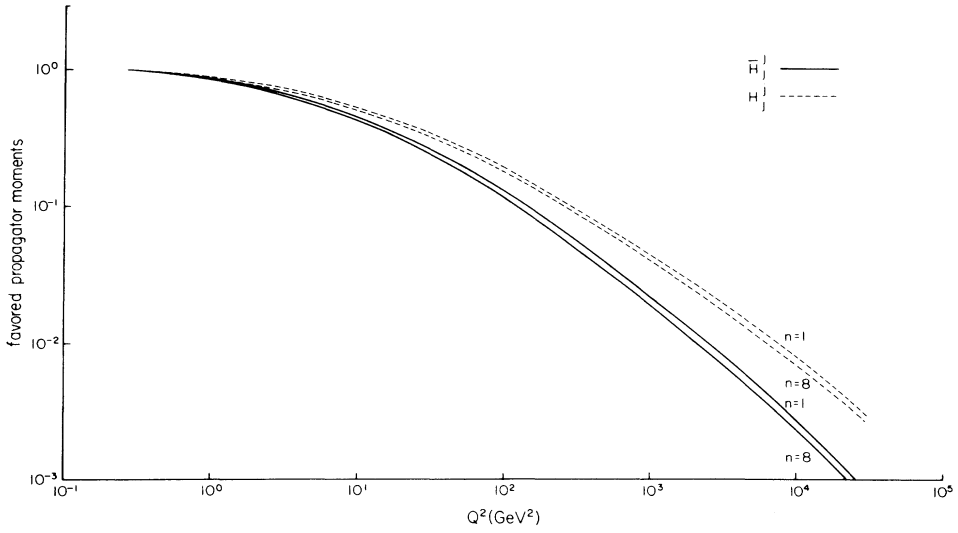

FIG. 8. Q^2 variation of the favored propagator moments for $n=1$ and $n=8$ (scheme A). $Q_0^2 = 0.062$ GeV^2.

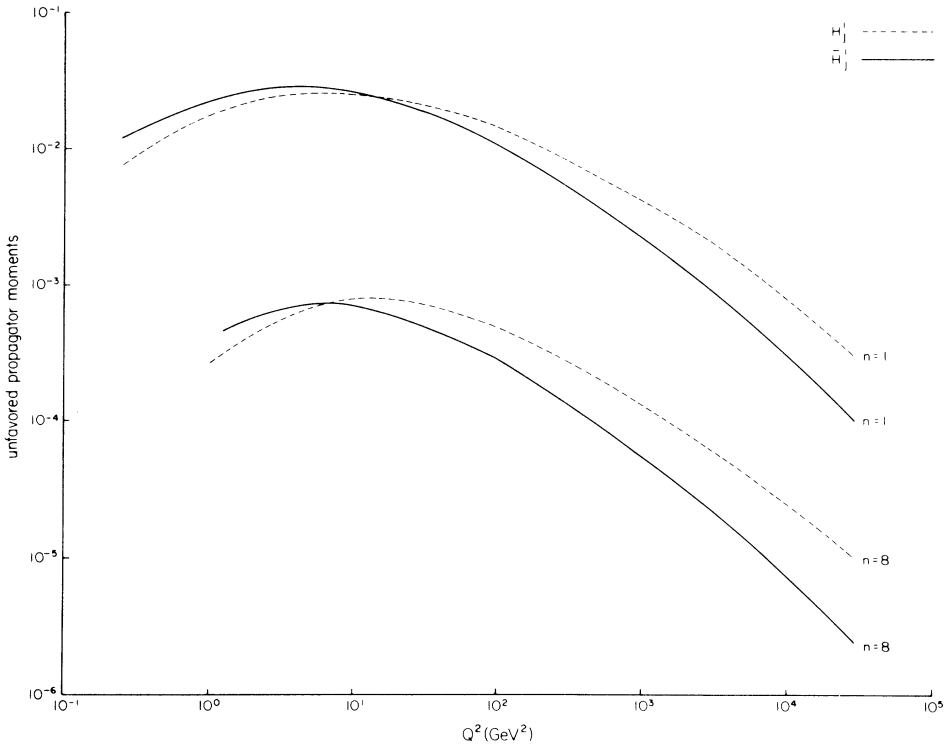

FIG. 9. Q^2 variation of the unfavored propagator moments for $n=1$ and $n=8$ (scheme A). $Q_0{}^2=0.062$ GeV^2.

where they are compared with the JM results. For the three kinds of propagators, as depicted in Figs. 8—10 where only the results of method A are shown, the difference between the incoherent and coherent analyses is more prominent at large Q^2 (the region of physical interest) where the present results (solid curve) are more damped.[19] The n dependence of the propagators is shown in Fig. 11 for a typical high $Q^2=3\times10^4$ GeV^2, where the calculations based on both methods A and B appear together with the JM results.

The favored propagator exhibits only a very small variation with n, for a given Q^2, which is reasonable since the

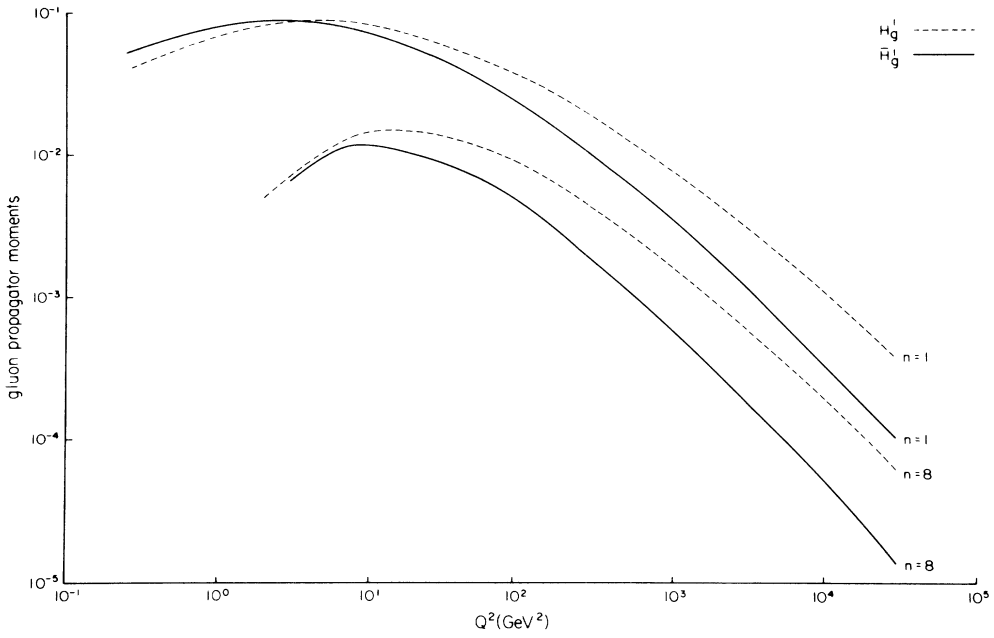

FIG. 10. Q^2 variation of the gluon propagator moments for $n=1$ and $n=8$ (scheme A). $Q_0{}^2=0.062$ GeV^2.

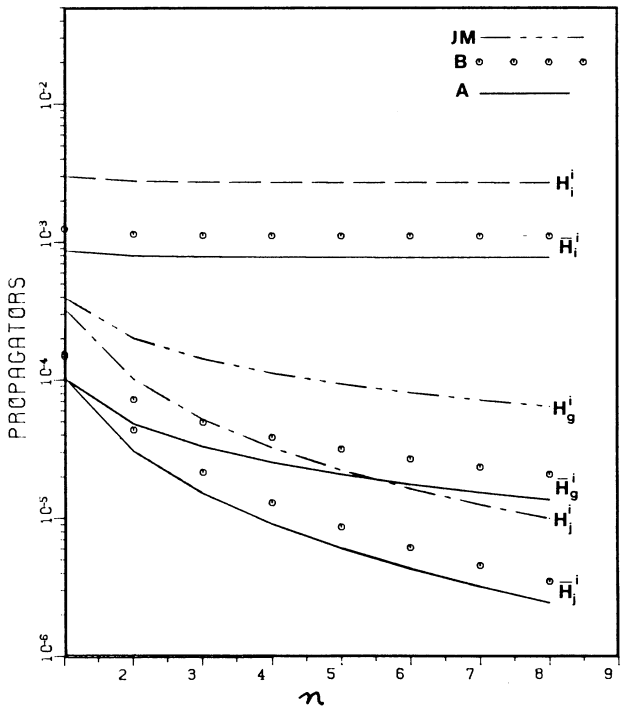

FIG. 11. Behavior of propagator moments as a function of n at $Q^2=30\,000$ GeV^2, $Q_0^2=0.062$ GeV^2.

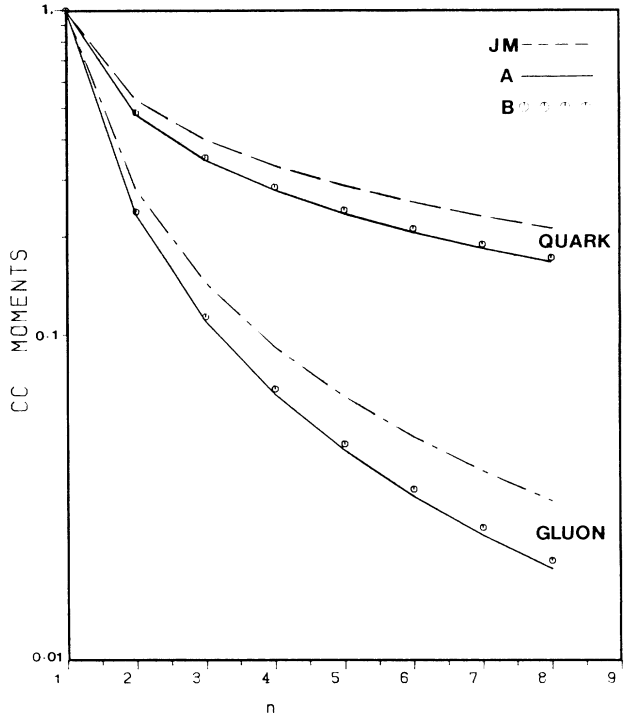

FIG. 12. Colorless-cluster moments [from Eqs. (2.4) and (3.15)] for incident quarks and gluons as a function of n at $Q^2=30\,000$ GeV^2, $Q_0^2=0.062$ GeV^2.

favored propagator moments are dominated by the $\delta(x-1)$ term; on the other hand, the unfavored and gluon propagators decrease as n increases in the three approaches. The results in the coherent scheme are more damped for higher n (by about 25% for the gluon propagator and 32% for the unfavored propagator, for $n=8$ compared to $n=1$). The results in the coherent B scheme are consistently larger than those in the A scheme by a factor not exceeding 1.6. (Obviously, this is also true for Figs. 8—10.) This is consistent with the observation made earlier in our discussion in Sec. IV D that the results of method B can differ from method A by a factor of at most 2, due to the very slow drop with P^2 of the results of the integrodifferential equations.

In Fig. 12 we show the results for the quark and gluon CS distribution moments. These moments are obtained by first solving for moments of Eq. (3.15) in terms of the $\tilde{H}$, and then averaging according to the techniques of Sec. IV. If one averages using the differential equation method of Sec. IV C, the entire set of differential equations is solved simultaneously for the $\tilde{H}$'s and the averaged output. The larger n moments are consistently lower than the JM results, the gap widening as n increases, for both quark and gluon distributions. There is an even smaller difference between methods A and B for the colorless-cluster moments, the ratio being 1.07 and 1.04 for gluon and quark, respectively.

B. Moment inversion

When we invert from moment space (where we know the calculated moments to reasonably high accuracy) to x space, we must choose a method for the inversion. This introduces systematic uncertainties, since we know only a finite number of moments (eight here); inversion methods which are guaranteed to work in the limit of infinite number of moments may not reproduce the function very accurately for small number of input moments.[17] In our past papers we have used the Yndurain inversion method, so there is some reason for us to present results here using it. This method has several drawbacks, however: (i) for eight moments we can only look for x above 0.2, thus the interesting low-x region is inaccessible; and (ii) Yndurain's method has been shown to be rather poor in reconstructing functions of this general shape when only eight moments are known. Counterbalancing these problems is an advantage: the Yndurain method is reasonably good at reproducing δ-function singularities near $x=1$, such as the one contained in the "favored" quark propagator; other methods used based on Legendre polynomials have a hard time with such singular behavior when only a few moments are known. (The Legendre approximation exhibits substantial oscillations.)

Most of the results that we present in this paper are obtained using the Yndurain inversion. Before we discuss these results from a physics point of view, we would like to give some idea of the systematic uncertainties involved in the inversion. Another inversion method, which has been shown to give good results for a small number of moments,[17] is based simply on an expansion in Legendre polynomials (see Appendix B). In Fig. 13 we show sample curves for colorless clusters in quark and gluon jets using our JM and "reconstructed" moments obtained with scheme A. We show results in x space based on both the

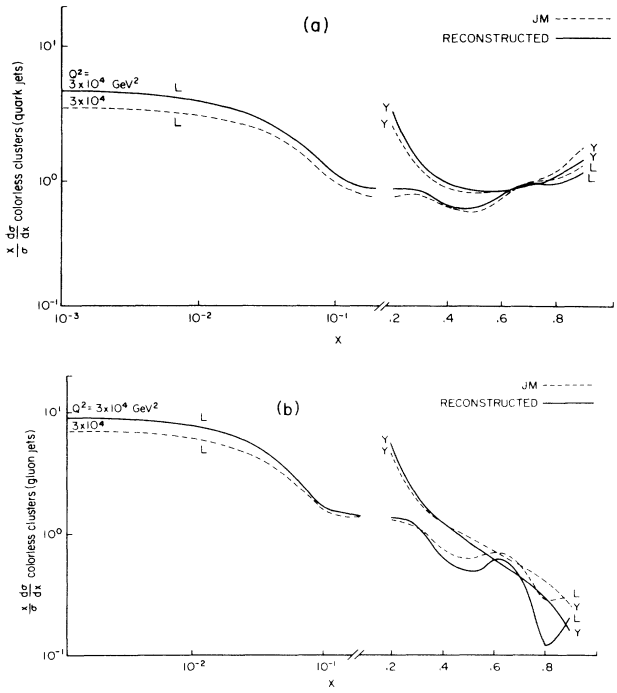

FIG. 13. Inversion of the moments shown in Fig. 12, showing discrepancy between the Legendre and Yndurain techniques: (a) quark; (b) gluon (scheme A).

Yndurain and Legendre inversion techniques; a logarithmic scale in x is used in order to emphasize the low-x region (the Legendre method yields a series which can be evaluated at any desired point).

Casual inspection of the curves shows that the two techniques do not yield the same x distributions in the region of overlap. The reader should take this as a warning about the overall quantitative meaning of the results. However, we see that both methods yield a "crossover point," and that the ordering of the curves (i.e., whether reconstructed is higher than JM or vice versa) below and above the crossover is the same for both inversion techniques.

We take this as an indication that certain qualitative features are correctly predicted even when only eight moments are known. These are the aspects of our calculation which should be compared with the Monte Carlo results of Marchesini and Webber.

C. Propagators in longitudinal momentum

The results for the propagators in x space are shown in Fig. 14. The favored propagator is much lower than that of JM, the gap increasing at higher Q^2. The δ function around $x=1$ is also somewhat damped. There is a tendency in all propagators to blow up at very low x; so we do not present results for x below 0.2.

In the case of the unfavored and gluon propagators, again we observe lower values. Notice that the favored and unfavored propagators are equal to each other except near $x=1$, as before. The softening of the δ function in the favored propagator causes the gluon propagator to drop at large x. Again, as expected, the propagators in x space obtained from method B are higher than those from method A by a factor of at most 1.6.

D. Colorless clusters

Although we can compute the Legendre series at arbitrarily small x, there is not much point here in a detailed examination of the very-low-x region. The reason for this is twofold: (i) our Crespi-Jones equations make some approximations in the kinematics which are not valid for very-slow (but finite-mass) particles, and (ii) we have not calculated the zeroth moment. A formula for the zeroth moment in the coherent branching scheme exists[11] and is the basis of various predictions about the multiplicity. Work including this in our scheme is underway. We have not included it here because our chief interest lies in the change between previous results and the new approach, and the more "old fashioned" jet calculus could not compute the zeroth moment (due to divergences). However, for x small but not "tiny," we do see the distribution go up as a result of angular ordering, in agreement with Ref. 13. There is also agreement in orders of magnitude.

Looking at the large-x region (Figs. 15 and 16 for methods A and B, respectively), there is a crossover around $x=0.7$ for the quark jets. We have calculated our moments accurately enough to verify that, indeed, this is really present. The inversion of the difference of the old and new moments yields a function which unambiguously changes sign. As discussed in Sec. V B above, we believe this crossover to be present even though different methods of moment inversion lead to slightly different values for the exact crossover point. A similar crossover phenomenon occurs for the gluon jets (Figs. 17 and 18), this time at a much lower x, about 0.5.

For both quark and gluon jets, the position of the crossover point is insensitive to the choice of reconstruction schemes (compare Figs. 15 and 16 with Figs. 17 and 18). This is because the scheme B and A results differ by at most 7% for gluon jets and 4% for quark jets.

We expect only very small deviations between the two schemes for these physical quantities because the moments vary very slowly with Q^2 (like powers of $\ln Q^2$). The fact that the results of the coherent branching lie above the old results at intermediate x and below them at high x agrees with the MW results, as does the direction of motion of the crossover point as Q^2 increases, for both quark and gluon jets. MW present results for gluon jets only.

VI. SUMMARY AND CONCLUSIONS

The angular ordering condition discovered by Mueller, which accounts for cancellations in the low-x region of phase space, can be reexpressed as a strong ordering in the variable $p^2=2\omega^2(1-\cos\theta_{12})$. This variable is approximately Lorentz invariant under boosts along the jet axis. As a result, jet-calculus-like integrodifferential equations determining the p^2 variation of all interesting quantities such as σ_g (the probability that gluons do not produce $q\bar{q}$ pairs), parton propagators, and colorless-cluster distribu-

tions can be written. These differ from the standard equations in q^2 in some crucial factors of $\frac{1}{2}$ due to the different low-z behavior of some important quantities and the obvious changes in the variable of integration.

We have solved these new equations, obtaining the P^2 dependence of various quantities. To compare these results of coherent branching with the older conventional jet-calculus results, we computed their consequences at particular values of Q^2 by averaging over the appropriate range of P^2. The procedure is effective in the sense that the small shifts between the "reconstructed" results and the "old" or "conventional" results are all in directions which can be interpreted simply in terms of physical distinctions between the two types of cascades. These results for the colorless clusters in both quark and gluon jets move up at intermediate x and down at large x, compared to "standard" jet-calculus calculations. These results for the physical quantities are independent of small corrections to the asymptotic kinematics. This is important in order that the jet calculus be useful. Our results are quite

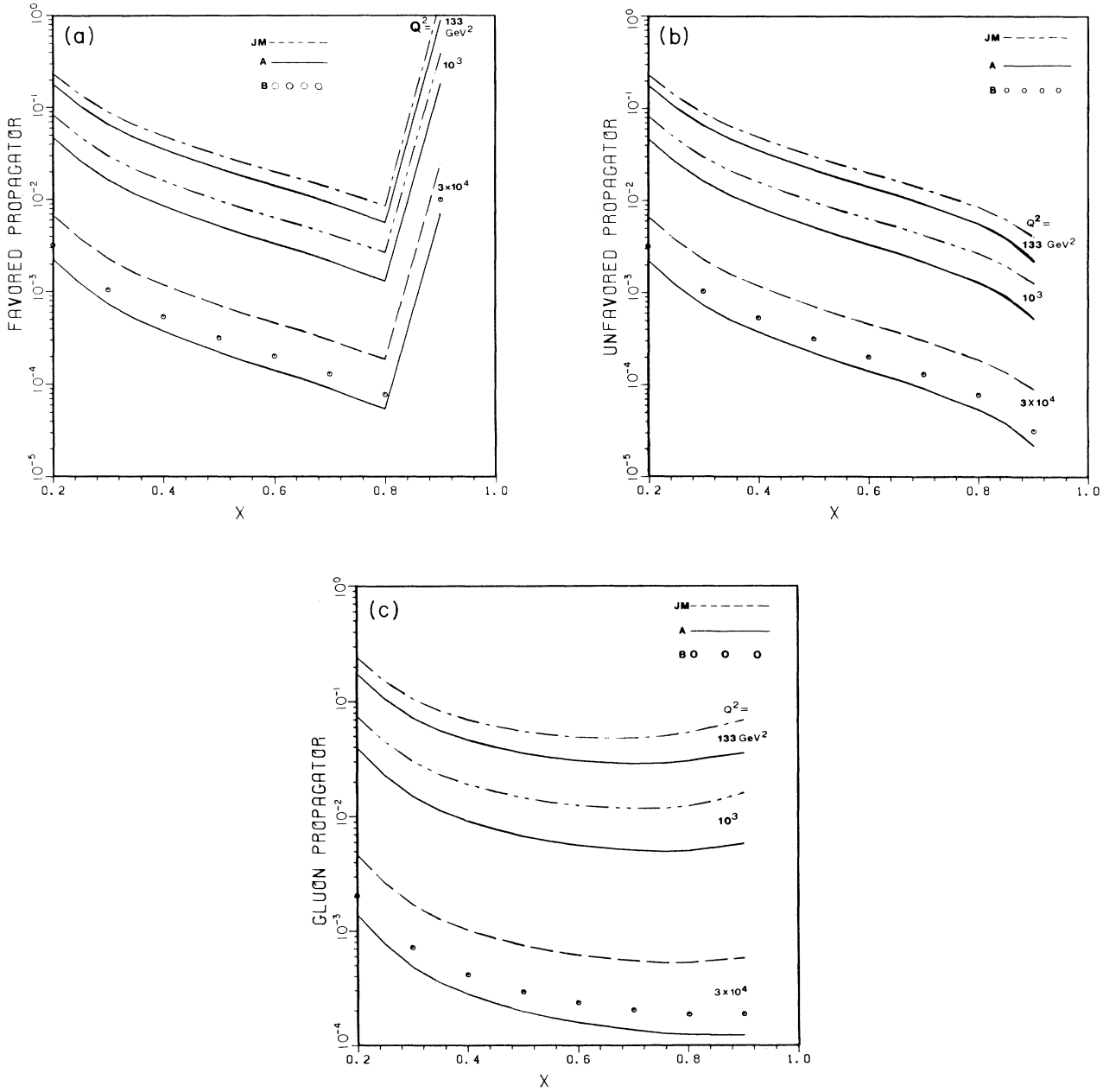

FIG. 14. Propagators as a function of x at different Q^2 ($Q_0{}^2=0.062$ GeV^2). (a) Favored propagator at $Q^2=133$, 1000, 30 000 GeV^2. (b) Unfavored propagator at the same Q^2 values. (c) Gluon propagator at the same Q^2 values.

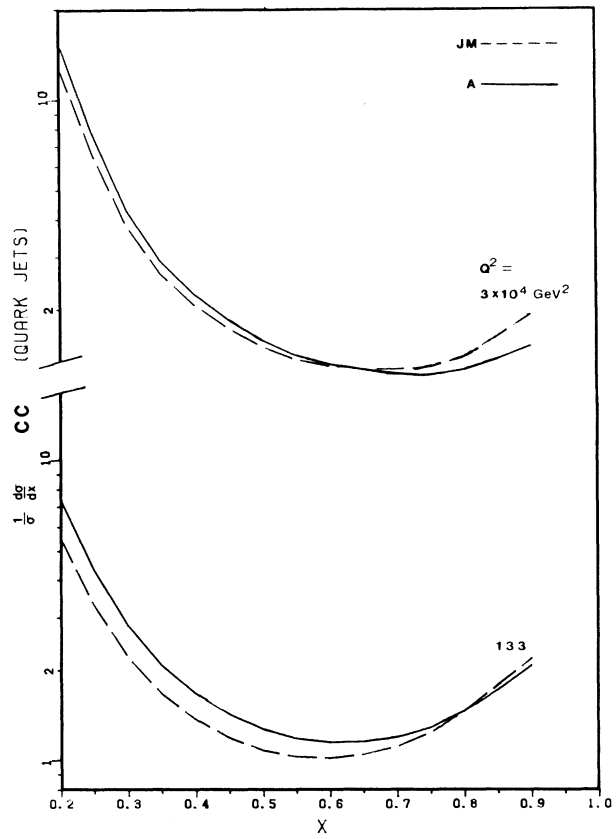

FIG. 15. CC distribution in quark jets at $Q^2=133$ and 30000 GeV^2. $Q_0^2=0.062$ GeV^2 (reconstruction A).

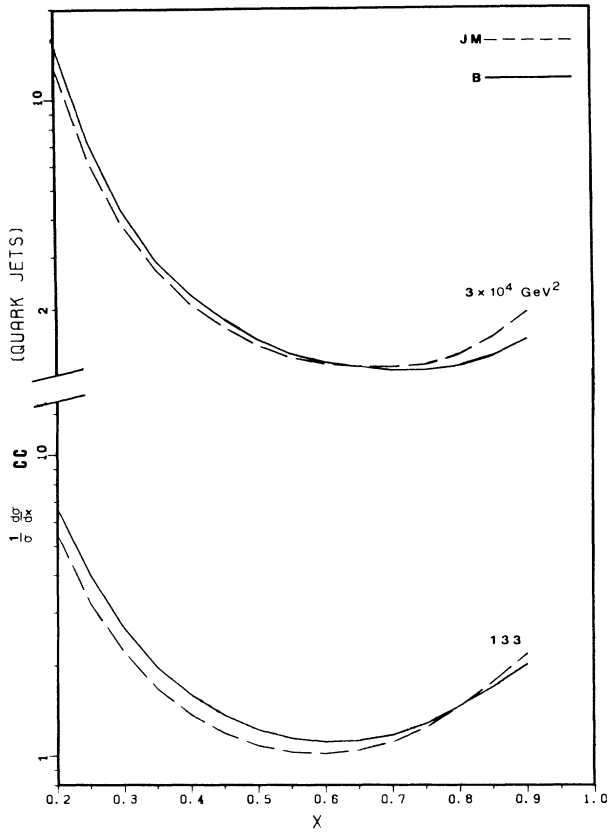

FIG. 16. CC distribution in quark jets at $Q^2=133$ and 30000 GeV^2. $Q_0^2=0.062$ GeV^2 (reconstruction B).

similar to those obtained by Marchesini and Webber in a Monte Carlo calculation of gluon jets with the same physics input.

We thus feel that there is no problem in incorporating the newly discovered effects of coherence into the jet-calculus equations. We are currently studying the extension of this approach to the zeroth moments, which will allow exploration of the interesting region at ultrasmall x.

ACKNOWLEDGMENTS

We gratefully acknowledge useful discussions with A. Bassetto, M. Ciafaloni, G. Marchesini, B. Crespi, and C.-K. Ng; we wish to thank A. Bassetto and B. R. Webber for their correspondence. We also wish to thank B. R. Webber and G. Marchesini for sending us their Monte Carlo program. This work was supported in part by DOE Contract No. DEACO 276 ERO 1195 (L.M.J.), NATO research Grant No. 779/83 (L.M.J. and R.M.), Natural Science and Engineering Research Council (NSERC) (Canada) operating Grant No. A9070 (R.M.), NSERC International Collaborative Research Grants (R.M.), and NSERC International Scientific Exchange Awards (L.M.J.).

APPENDIX A: KINEMATICS

First we consider the branching in the conventional scheme [Fig. 5(a)]:

$$q^2=\frac{q_1^2+p_t^2}{z}+\frac{q_2^2+p_t^2}{1-z}\quad (q_1^2,q_2^2\geq Q_0^2)\ . \tag{A1}$$

Using

$$p_t^2=z(1-z)q^2-(1-z)q_1^2-zq_2^2 \tag{A2}$$

we get

$$z(1-z)q^2\geq(1-z)q_1^2+zq_2^2\geq Q_0^2\ . \tag{A3}$$

So, generally speaking,

$$z(1-z)\geq\frac{Q_0^2}{q^2}\ .$$

Hence, as we know from ordinary kinematics,

$$q_{\min}^2=4Q_0^2\ .$$

When integrating over z, we use the large-q^2 approximation:

$$z_-=\frac{Q_0^2}{Q^2}$$

and (A4)

$$z_+=1-\frac{Q_0^2}{Q^2}\ .$$

Next we consider the coherent branching mechanism:

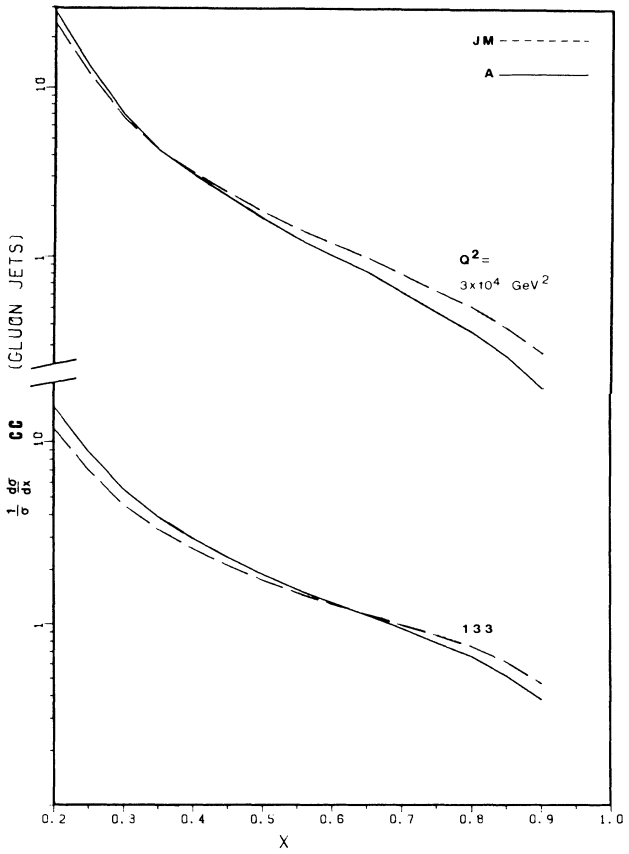

FIG. 17. CC distribution in gluon jets at $Q^2=133$ and 30 000 GeV^2. $Q_0{}^2=0.062$ GeV^2 (reconstruction A).

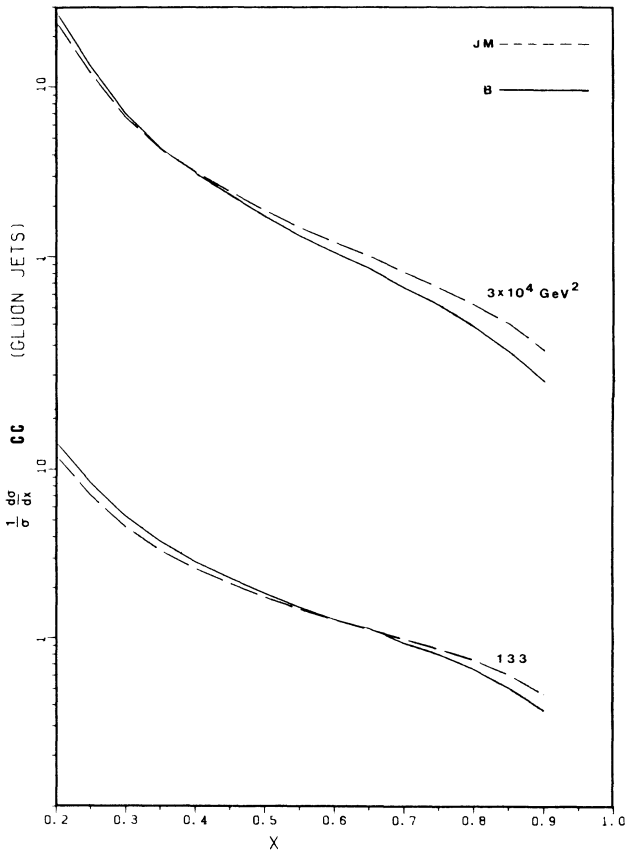

FIG. 18. CC distribution in gluon jets at $Q^2=133$ and 30 000 GeV^2. $Q_0{}^2=0.062$ GeV^2 (reconstruction B).

since $p_t{}^2>0$, and

$$q^2=q_1{}^2+q_2{}^2+q_2{}^2+z(1-z)p^2 ,$$

we find

$$P^2z^2(1-z)^2\geq Q_0{}^2[z^2+(1-z)^2] . \tag{A5}$$

The function

$$\frac{z^2(1-z)^2}{z^2+(1-z)^2}\geq\frac{Q_0{}^2}{P^2} \tag{A6}$$

has a maximum again at $\frac{1}{2}$. Thus $(P^2)_{\min}=8Q_0{}^2$.

At large P^2 this leads to limits

$$z_-=\frac{Q_0}{P}$$

and (A7)

$$z_+=1-\frac{Q_0}{P} .$$

APPENDIX B: THE LEGENDRE METHOD OF INVERSION (REF. 17)

In this appendix we present a summary of the Legendre inversion technique discussed in Ref. 17, and used to prepare Fig. 13.

Let $f(x)$ be the "true," unknown function and

$$\bar{f}(n)=\int_0^1 dx\, x^n f(x) \tag{B1}$$

its nth moment, where $n=1,2,\ldots,N$. The Legendre method allows us to reconstruct the value of the function at any desired x from a set of $\bar{f}(n)$, $n=1,\ldots,N$. This involves an expansion in Legendre polynomials P_l. Explicitly, if

$$P_l(y)=\sum_{i=0}^{l}c_i^l y^i$$

then the inversion is achieved by means of the formula

$$f_L(x)=\frac{1}{x}\sum_{l=0}^{N-1}(2l+1)P_l(2x-1)\sum_{i=0}^{l}c_i^l\sum_{m=0}^{i}\binom{i}{m}2^m(-1)^{i-m}\bar{f}(m+1) , \tag{B2}$$

where $f_L(x)$ is the resulting approximation to $f(x)$.

In our solution of the differential equations the moments were calculated to an accuracy of one part in 10^8. We calculate eight moments for inversion. As discussed in Ref. 17, these values for the error and the number of moments are optimally matched, in the sense that they reproduce test functions more accurately than would a larger number of moments known to 1 part in 10^8.

---

[1]B. L. Ioffe in *Proceedings of the 22nd International Conference on High Energy Physics,* Leipzig, 1984, edited by A. Meyer and E. Wieczorek (Akademie der Wissenschaften, Zeuthen, East Germany, 1984), Vol. 2, p. 176.

[2]M. Jacob, in *Proceedings of the 22nd International Conference on High Energy Physics* (Ref. 1), p. 150.

[3]S. D. Ellis, in *Dynamics and Spectroscopy at High Energy,* proceedings of the 11th SLAC Summer Institute on Particle Physics, Stanford, 1983, edited by P. M. McDonough (SLAC Report No. 267, 1984).

[4]G. Altarelli and G. Parisi, Nucl. Phys. **B126**, 298 (1977).

[5]K. Konishi, A. Ukawa, and G. Veneziano, Nucl. Phys. **B157**, 45 (1979).

[6]D. Amati and G. Veneziano, Phys. Lett. **83B**, 87 (1979).

[7]A. Bassetto, M. Ciafaloni, and G. Marchesini, Nucl. Phys. **B163**, 477 (1980).

[8]B. Crespi and L. M. Jones, Phys. Rev. D **28**, 2840 (1983).

[9]L. M. Jones and R. Migneron, Phys. Rev. D **27**, 2715 (1983).

[10]D. Amati, A. Bassetto, M. Ciafaloni, G. Marchesini, and G. Veneziano, Nucl. Phys. **B173**, 429 (1980).

[11]A. H. Mueller, Phys. Lett. **104B**, 161 (1981); Nucl. Phys. **B213**, 85 (1983). For a recent rederivation of the angular ordering, see R. Kirschner, in *Proceedings of the 22nd International Conference on High Energy Physics* (Ref. 1), p. 98.

[12]A. Bassetto, M. Ciafaloni, G. Marchesini, and A. H. Mueller, Nucl. Phys. **B207**, 189 (1982); Yu. L. Dokshitzer, V. S. Fadin, and V. A. Khoze, Phys. Lett. **115B**, 242 (1982); A. Bassetto, M. Ciafaloni, and G. Marchesini, Phys. Rep. **100**, 201 (1983).

[13]G. Marchesini and B. R. Webber, Nucl. Phys. **B238**, 1 (1984) (hereafter referred to as MW); G. Marchesini, Acta Phys. Pol. **B15**, 277 (1984); B. R. Webber *ibid.* **B15**, 617 (1984); M. Ciafaloni, in *Proceedings of HEP83,* International Europhysics Conference, Brighton, England, 1983, edited by J. Guy and C. Costain (Rutherford Laboratory, Chilton, England, 1983), p. 199; B. R. Webber, CERN Report No. CERN-TH-3713, 1983 (unpublished).

[14]After this paper was first submitted for publication, two other works discussing angle ordering have been circulated, R. Odorico (unpublished) and T. Gottschalk, Report No. CALT-68-1333 (unpublished). Neither of these uses a jet-calculus approach.

[15]A. V. Kiselev, IHEP Report No. 83-56, 1983 (unpublished).

[16]F. J. Yndurain, Phys. Lett. **74B**, 68 (1978).

[17]L. M. Jones and L. R. Opsahl, J. Phys. G **12**, 591 (1986).

[18]We found that the accuracy in the integration was greatly improved by changing the variable of integration from P^2 to $\ln P^2$; this is important for the purpose of moment inversion.

[19]As a check on self-consistency in both the solution procedure of the system of differential equations and the reconstruction schemes outlined earlier, the results for σ_g and the various propagators are shown at very low Q^2 in Figs. 6—10. The favored propagator is well behaved down to the boundary at $4Q_0^2$ in both schemes. For both the unfavored and gluon propagator moments, as Q^2 decreases, a maximum is reached in both schemes, from which the curves tend to drop off as the boundary $4Q_0^2$ is approached. The behavior near the boundary is consistent with the boundary conditions imposed on the propagators.